JOC The Journal of Organic Chemistry

Article

pubs.acs.org/joc

Axial Coordination Dichotomy in Dirhodium Carbenoid Catalysis: A Curious Case of Cooperative Asymmetric Dual-Catalytic Approach toward Amino Esters

Hemanta K. Kisan and Raghavan B. Sunoj*

Department of Chemistry, Indian Institute of Technology Bombay, Powai, Mumbai 400076, India

Supporting Information

ABSTRACT: One of the most recent developments in asymmetric catalysis is to employ two or more catalysts under one-pot reaction conditions. This article presents some interesting mechanistic insights on a cooperative dual-catalytic protocol relying on the catalytic ability of dirhodium carbenoid (derived from rhodium(II) tetracarboxylate and a diazo compound) and a chiral spirophosphoric acid ((*R*)-SPA) in an asymmetric N−H insertion reaction. We have employed DFT(M06 and B3LYP) computational methods to identify the stereocontrolling transition states wherein a chiral (*R*)-SPA protonates a dirhodium-bound enol intermediate. A true cooperative action elicited by both catalysts has been noted in the enantioselective protonation. More importantly, whether the second axial ligand on the remote rhodium atom could influence the energetic features of the reaction has been probed for the first time. In all steps (such as nitrogen extrusion, addition of amine to the dirhodium carbenoid, and the enol formation), except that in the stereocontrolling event, no major effect of axial ligation has been noticed. However, the presence of the axial ligand helps in stabilizing the protonation transition state and reduces the activation barrier for protonation, suggesting a vital role in stereoselectivity. The predicted sense of stereoselectivities is in good agreement with the experimental results.

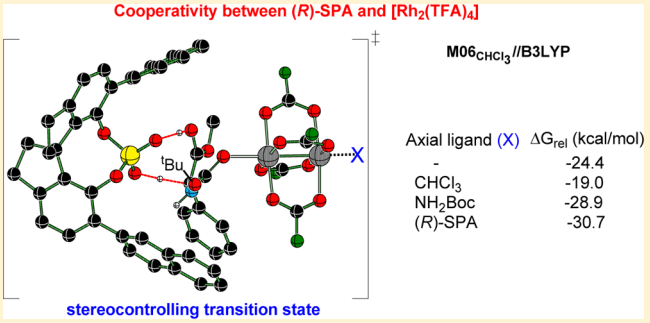

INTRODUCTION

The chemistry of dirhodium(II) carboxylates came to the forefront owing to the catalytic potential of the corresponding dirhodium carbenoids.[1] A whole gamut of reactions, such as X−H insertion (where X = C, N, O, S), cyclopropanation, C−H functionalization, cycloadditions, ring-expansion, and so on have become available over the years. The mechanism of dirhodium carbenoid catalysis has garnered considerable interest and led to a series of debates since its inception. Questions such as whether the nitrogen extrusion involved in the generation of dirhodium carbenoid is the rate-limiting step[2] and whether the lantern-like tetraacetate structure remains intact or it allows ligand exchanges under catalytic conditions have been addressed.[3] While these two issues appear nearly settled, the legacy debate on diaxial coordination continues to remain fresh.

It is generally expected that the electrophilic rhodium centers bind to other molecules present in the medium. There have been a number of X-ray crystallographic demonstrations that indicate both rhodium atoms could bind to ligands of varying donating abilities. A selected set of X-ray structures that exhibit diaxial coordination are (a) extended 1D and 2D structures by $Rh_2(O_2CCF_3)_4$ linked through polycyclic aromatic hydrocarbons,[4] (b) 2D network of fullerene and $Rh_2(O_2CCF3)_4$,[5] (c) binding of DMAP molecules to each rhodium atom of a *tert*-leucine-derived dirhodium catalyst,[6] (d) binding of N-heterocyclic carbenes to $Rh_2(O_2CCH_3)_4$,[7] and (e) weaker coordination of chloromethane[8] as well as acetonitrile[9] to $Rh_2(tpa)_4$. Although diaxial coordination of ligands to the dirhodium framework is well-established in the solid state, the scenario may be quite different in the condensed phase typically employed in a catalytic reaction.

In fact, measurement of equilibrium constants in solution for the binding of various ligands to dirhodium acetates has triggered a series of questions on the very premise of diaxial coordination. In an early report, Drago and co-workers have shown that the coordination of a second acetonitrile at the axial positions of dirhodium(II) tetrabutyrate in a 1:2 adduct is about 3 orders of magnitude weaker than that in 1:1 adduct.[10] Similarly, kinetic studies by Pirrung revealed that the active dirhodium catalyst uses only one of its coordination sites while engaging in catalysis.[11] This would imply that only one carbenoid per molecule of catalyst is possible, leaving the other site open. Strong binding with the carbenic carbon is expected to disfavor binding of other ligands to the second rhodium. It is also important to note that Doyle and co-workers[9] showed that the equilibrium constant for association of a second acetonitrile molecule exhibited significant variations depending on the nature of the bridging acetate ligands. Another study relevant to

Received: November 28, 2014
Published: February 2, 2015

DOI: 10.1021/jo5027029
J. Org. Chem. 2015, 80, 2192−2197

the present thesis is an interesting catalytic arylation of aldehydes by dirhodium acetate reported by Gois and co-workers.[7] On the basis of their mass spectroscopic analysis, a mono-NHC ($(NHC)Rh_2(OAc)_4$) was suggested as the precatalyst from which the carbenoid can be derived. Thus, the diverse range of experimental observations documented to date on the issue of diaxial coordination indiate that although weak the second ligand coordination could not be fully discounted. In other words, the effect of diaxial coordination on catalysis warrants careful molecular level scrutiny.

A more recent application of dirhodium carbenoid chemistry is in asymmetric catalysis using chiral bridging ligands. Earlier, Doyle noted that enantiomeric excess was unaffected by the presence of acetonitrile while the use of stronger donors such as pyridine resulted in lack of product formation in a [3 + 3] cycloaddition reaction catalyzed by a dirhodium carboxylate.[12] Charette and co-workers have noted enhanced enantioselectivity in an asymmetric cyclopropanation reaction in the presence of DMAP as compared to its absence.[13] In a dirhodium catalyzed diastereoselective amination reaction, additives have been demonstrated to impact the observed stereochemical course of the reaction.[6] Along these lines, efforts have also been expended to fine-tune the catalytic properties of dirhodium complexes by exploiting weak axial coordination.[14]

In line with the emerging trends in catalysis, dirhodium cabenoid is now being used in conjunction with other catalysts under one-pot reaction conditions. Such homogeneous multicatalytic reactions present formidable challenges toward its mechanistic understanding.[15] In one such elegant dual-catalytic strategy, an asymmetric N−H insertion reaction was very recently reported wherein the dirhodium carbenoid is achiral.[1g] The source of chirality is provided through an *external* spirophosphoric acid (Brønsted acid catalysis). The reaction, as shown in Scheme 1, represents an interesting class of dual

Scheme 1. Cooperative Catalysis by Dirhodium(II) Tetra(trifluoroacetate) [$Rh_2(TFA)_4$] and Chiral Spinol Phosphoric Acid ((*R*)-SPA) in an Asymmetric N−H Insertion Reaction

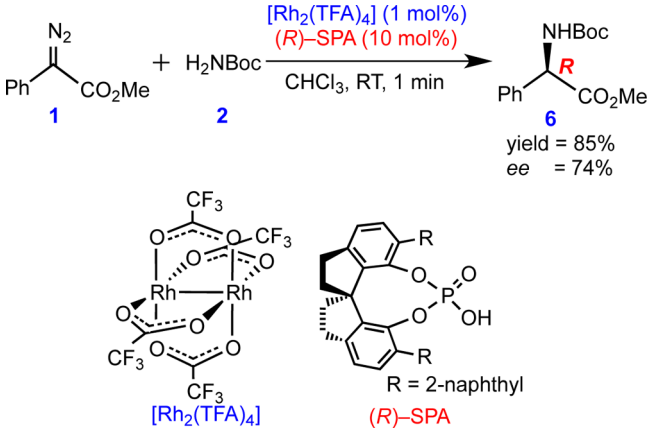

catalytic approach leading to a chiral α-amino ester. Through a recent communication, we have established the mechanism of this reaction, without any axial ligands on the catalyst. It has been identified that the enantioselective step involves a dual proton transfer promoted by the spinol phosphoric acid ((*R*)-SPA).[16] In this article, we intend to evaluate the effect of axial coordination on various elementary steps involved in the catalytic cycle in general and on the stereoselective proton transfer in particular. The density functional theory computations in the condensed phase (chloroform) using the M06 functional are employed in the present study. The geometries have been optimized at the B3LYP/LanL2DZ(Rh),6-31G* level of theory.

COMPUTATIONAL METHODS

All computations were carried out using the Gaussian 09 suite of quantum chemical program.[17] The hybrid density functional B3LYP was used for geometry optimization of all the stationary points, which includes intermediates, reactants, and transition states.[18] The Los Alamos pseudopotential basis set (LanL2DZ) was used for rhodium (Rh), consisting of effective core potential (ECP) for 28 inner electrons for rhodium (Rh) and Pople's 6-31G* basis set for the remaining elements.[19] Frequency calculations were done on all the stationary points so as to characterize them as minima or transition states. The transition states (TSs) were characterized, first by visual inspection of the atomic displacement vectors that appear as one and only one imaginary frequency of the desired reaction coordinate. All other minima were characterized by a Hessian index of zero. Intrinsic reaction coordinate (IRC) calculations were carried out on the transition states to ascertain that the transition states obtained connect to the reactants and the products on either side of the first order saddle point.[20] The end-point geometries obtained through the IRC calculation were subjected to further optimization using a more stringent criteria by the "opt = calcfc" option which connects reactant and product to the transition state.

The effect of solvent was incorporated using the continuum solvation model SMD developed by Truhlar and Cramer.[21] The reaction was conducted in chloroform ($CHCl_3$), and hence, we have used the continuum dielectric of chloroform (ε = 4.81) in our computations in the condensed phase. The single-point energies of all the stationary points were obtained at the $SMD_{(Chloroform)}$/M06/LanL2DZ(Rh),6-31G**(C,H,N,O,F,P,Cl)//B3LYP/LanL2DZ(Rh),6-31G*(C,H,N,O,F,P,Cl) level of theory. The Gibbs free energies and enthalpies for all stationary points in the condensed phase were obtained by adding the zero-point vibrational energy (ZPVE), thermal and entropic corrections obtained from the gas-phase computations. The results and discussion are presented on the basis of the Gibbs free energies in the solvent. Natural bond orbital (NBO) analysis was carried out at the B3LYP/LanL2DZ(Rh),6-31G**(H,C,N,O,F,P,Cl) level of theory on a few stereodetermining transition states.[22]

RESULTS AND DISCUSSION

The important steps involved in the catalytic cycle are summarized in Scheme 2. The mechanism can be broadly viewed as consisting of two key events, namely, the generation of a dirhodium carbenoid intermediate and an enantioselective protonation of the ensuing enol intermediate leading to a chiral carbon atom. The initial activation of the diazocompound (**1**) is followed by nitrogen extrusion, which is generally proposed to be rate-limiting step.[2] The resulting dirhodium carbenoid **3** will be intercepted by the nucleophile H_2NBoc to provide a zwitterionic intermediate **4**. An intramolecular proton transfer in **4** leading to an enol intermediate **5** is found to be energetically more favored over the alternative possibilities such as the generation of an enolate or a ylide through a change of coordination of the rhodium from the carbon to the carbamate oxygen.[16] The enol intermediate **5** is the most important species in the catalytic cycle, which can be protonated on either of the prochiral faces (*re* or *si*) to give the amino ester (**6**) as the final product. It should be noted that a free enol as well as a $Rh_2(TFA)_4$ bound enol are both achiral and hence no stereoinduction is expected. Simple protonation would lead only to a racemic mixture. Hence, the protonation should

DOI: 10.1021/jo5027029
J. Org. Chem. 2015, 80, 2192−2197

Scheme 2. Key Steps in $[Rh_2(TFA)_4]$-Catalyzed Reaction between Diazoacetate and *tert*-Butyl Carbamate

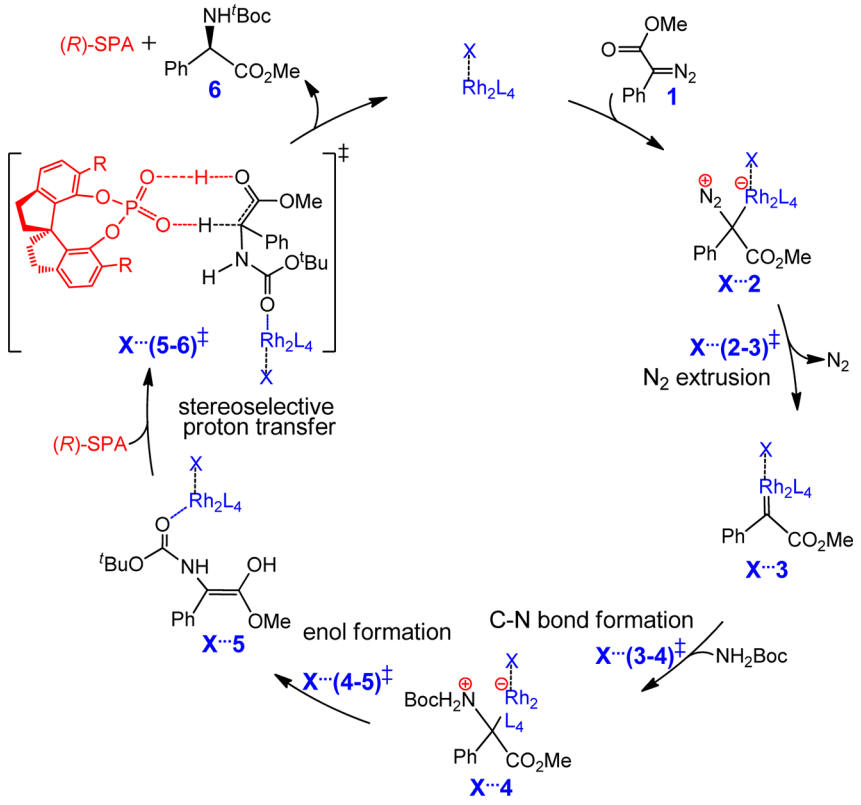

involve chiral spinolphosphoric acid such that it can impart enantioselectively.

Under a condensed-phase catalytic condition, the timing and mode of action of catalyst on each reactant is not quite clear. Hence, the effect of coordination of various available ligands to the vacant site of dirhodium acetate is considered in this study. In the present dual-catalytic scenario, (*R*)-SPA, H_2NBoc, or even the solvent $CHCl_3$ could occupy the axial position of dirhodium tetracarboxylate. The relative Gibbs free energies are computed with and without axial ligands for various elementary steps (Table 1). The Gibbs free energies are employed for discussion as it includes molecular entropy changes.

A careful examination of the relative energies of important intermediates and the interconnecting transition states, as summarized in Table 1, conveys some interesting features of this reaction. In general, binding to axial ligands exerts some effect on the stabilization of both transition state and the preceding intermediate involved in each step. The elementary step barriers for each step are calculated as the difference in Gibbs free energies between the transition state and its preceding intermediate. The most notable effect, in the form of additional stabilization, is offered by (*R*)-SPA at the axial position. It is interesting to note that the Gibbs free energy of the transition state is 2.6 kcal/mol lower with an axial (*R*)-SPA as compared to its absence in the nitrogen extrusion step (see Table 1, $(2-3)^‡$ versus **(*R*)-SPA···$(2-3)^‡$**, and see Figure 1 for the optimized geometry of the latter). However, the activation barrier with axial ligation is higher by 1.8 kcal/mol. It is important to recall that the expulsion of nitrogen from the diazo compound has generally been regarded as the rate-determining step in literature.[2] Similarly, axial coordination of H_2NBoc in transition state $(2-3)^‡$ only serves to result in a modest increase in the activation barrier.

A similar trend holds true in the next step of the catalytic cycle wherein the nucleophilic addition of H_2NBoc to the dirhodium carbenoid intermediate (**3**) takes place. In fact, the transition state $(3-4)^‡$ for the C−N bond formation prefers no axial ligation, as it results in destabilization as well as an accompanying increase in the barrier. This could be rationalized by the fact that the coordination of an electron rich ligand at the axial site would result in lowering of electrophilicity of the carbenic carbon atom.[2a,7b,11−13,23] Similarly, the enolization step via the transition state $(4-5)^‡$ experiences little effect due to the presence of an axial ligand. On the basis of the computed barriers, it is evident that stronger ligands such as (*R*)-SPA and H_2NBoc produce kinetically unfavorable effect in the nitrogen extrusion, nucleophilic addition, and enolization steps.

Table 1. Computed Relative Gibbs Free Energies[a] (in kcal/mol) of the Key Intermediates and the Transition States with Different Axial Ligands (X)

stationary points	X = −	X = (*R*)-SPA	X = NH_2Boc	X = $CHCl_3$
X···$[Rh_2(TFA)_4]$	*b*	−8.0	−8.4	2.8
X···2	−2.7	−7.1	−6.7	3.1
X···$(2-3)^‡$	5.4	2.8	3.6	10.8
X···3	−18.5	−18.9	−16.8	−13.7
X···$(3-4)^‡$	−15.7	−14.0	−12.3	−10.3
X···4	−30.7	−35.9	−30.0	−24.1
X···$(4-5)^‡$	−26.4	−27.8	−26.0	−21.9
X···5	−27.7	−29.5	−32.1	−20.7

[a]The relative Gibbs free energies at the $SMD_{(chloroform)}$/M06/LanL2DZ(Rh),6-31G**(H,C,N,O,F,P,Cl)//B3LYP/LanL2DZ(Rh),6-31G*(H,C,N,O,F,P,Cl) level of theory are computed with respect to the separated reactants. [b]Not applicable.

DOI: 10.1021/jo5027029
J. Org. Chem. 2015, 80, 2192−2197

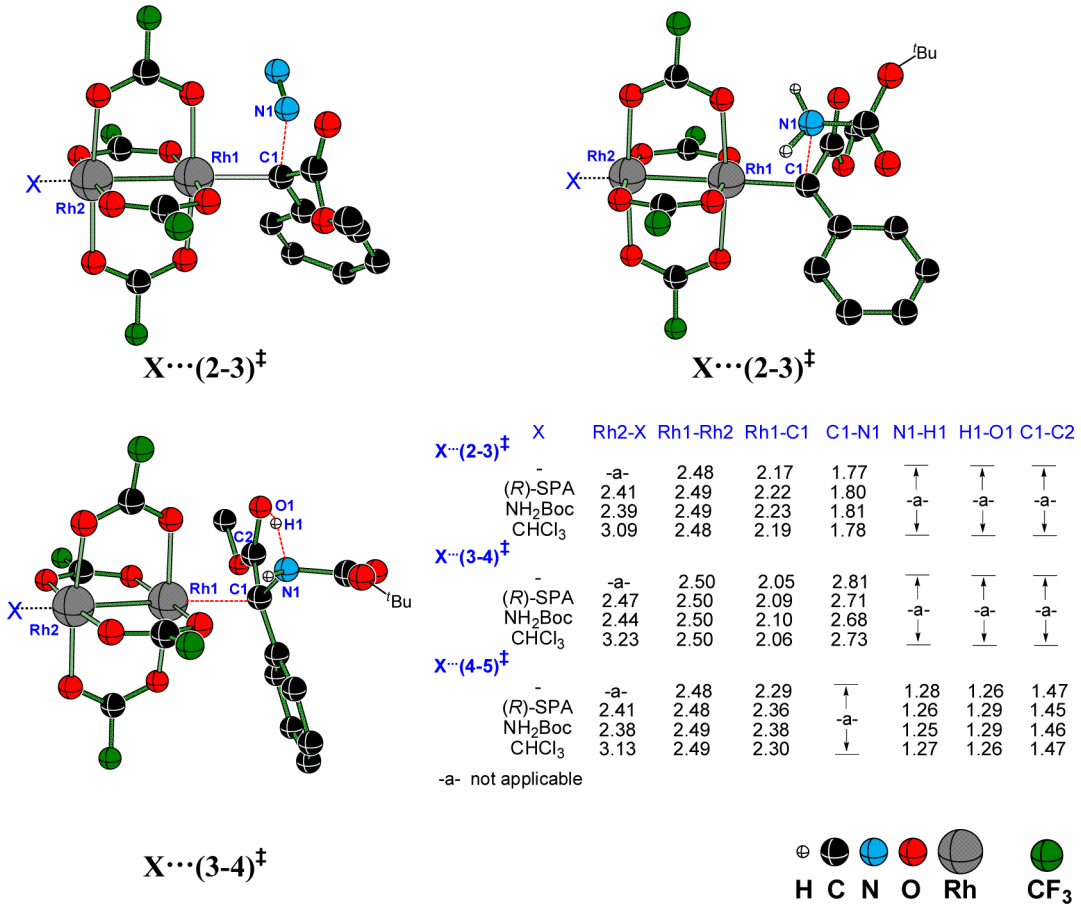

	X	Rh2-X	Rh1-Rh2	Rh1-C1	C1-N1	N1-H1	H1-O1	C1-C2
X···(2-3)‡								
	-	-a-	2.48	2.17	1.77			
	(*R*)-SPA	2.41	2.49	2.22	1.80			
	NH_2Boc	2.39	2.49	2.23	1.81	-a-	-a-	-a-
	$CHCl_3$	3.09	2.48	2.19	1.78			
X···(3-4)‡								
	-	-a-	2.50	2.05	2.81			
	(*R*)-SPA	2.47	2.50	2.09	2.71			
	NH_2Boc	2.44	2.50	2.10	2.68	-a-	-a-	-a-
	$CHCl_3$	3.23	2.50	2.06	2.73			
X···(4-5)‡								
	-	-a-	2.48	2.29		1.28	1.26	1.47
	(*R*)-SPA	2.41	2.48	2.36		1.26	1.29	1.45
	NH_2Boc	2.38	2.49	2.38	-a-	1.25	1.29	1.46
	$CHCl_3$	3.13	2.49	2.30		1.27	1.26	1.47

-a- not applicable

Figure 1. Optimized geometries of the transition states for N_2 extrusion (X···(2−3)‡), C−N bond formation (X···(3−4)‡) and enol formation (X···(4−5)‡) where X is 0(Nil), $CHCl_3$, NH_2Boc, and (*R*)-SPA. The distances are in angstroms optimized at the $SMD_{(chloroform)}$/M06/LanL2DZ(Rh),6-31G**//B3LYP/LanL2DZ(Rh),6-31G* level of theory. Only selected C and H are shown.

After evaluating the mechanistic features up until the formation of the enol intermediate (**5**), we turned our attention to the stereocontrolling event of the catalytic cycle. One can envisage a few likely scenarios in the stereoselective protonation. It was earlier reported that the protonation of a free enol by (*R*)-SPA is of higher energy by about 7 kcal/mol as compared to the protonation of a dirhodium-bound enol.[16] Further, in the most preferred mode for protonation, the dirhodium prefers to bind to the carbonyl oxygen of the H_2NBoc group as opposed to the alternative sites such as the aryl group or the nitrogen atom of the enol moiety. The enantioselective protonation is identified to involve a relay proton transfer between the phosphoric acid and the enol. The protonation of the prochiral carbon by the phosphoric acid is found to be accompanied by the abstraction of the enol proton by the incipient phosphate at the other end as shown in Figure 2. This relay proton transfer is evident through the optimized geometries of both the diastereomeric transition states ***si*-(5−6)‡···X** and ***re*-(5−6)‡···X**.[24] The *si* and *re* notations in these transition states, respectively, refer to the prochiral faces of the enol, which gets protonated. It can be readily noticed that both catalysts, namely (*R*)-SPA and $Rh_2(TFA)_4$, are directly involved in the stereocontrolling event, which is a testimony to true cooperative mode of catalysis. The intriguing question at this juncture is whether the enol-bound dirhodium prefers to leave the axial coordination open or would exhibit any effect upon coordinating with a ligand. To address this question, the computed relative Gibbs free energies for enantioselective protonation are provided in Table 2.

Certain interesting features are conspicuous from the relative free energies as provided in Table 2. First, there is a noticeable stabilization of the proton-transfer transition states when (*R*)-SPA occupies the axial position. The Gibbs free energy of ***si*-(5−6)‡···(*R*)-SPA** is about 6 kcal/mol lower as compared to ***si*-(5−6)‡** devoid of any axial ligand. The activation barrier, with respect to the preceding intermediate **5···(*R*)-SPA** is lowered by 4.5 kcal/mol due to axial ligation. Other axial ligands are not as effective as (*R*)-SPA. A similar trend is followed in the protonation of the *re*-face of the dirhodium-enol with an axial (*R*)-SPA. The most preferred mode of protonation is identified as the one wherein the *si*-face of the dirhodium-enol is protonated. Such a mode of protonation leads to an *R* enantiomer as the final product. The Gibbs free energy difference between the transition states ***si*-(5−6)‡···(*R*)-SPA** and ***re*-(5−6)‡···(*R*)-SPA** is about 6.7 kcal/mol that corresponds to an enantiomeric excess of more than 99%, which is in good agreement with the experimental value.[1g,16]

The optimized geometries of the sterecontrolling transition states, as given in Figure 2, convey that the interaction of the enol moiety with the dirhodium core is affected by the axial ligand (X) on the other rhodium center. For instance, a weak ligand such as chloroform does not render any structural change, such as in the Rh1−Rh2 distance of the dirhodium acetate framework. Axial ligands such as (*R*)-SPA and H_2NBoc result in an elongation of the O1−Rh1 distance. While the

DOI: 10.1021/jo5027029
J. Org. Chem. 2015, 80, 2192−2197

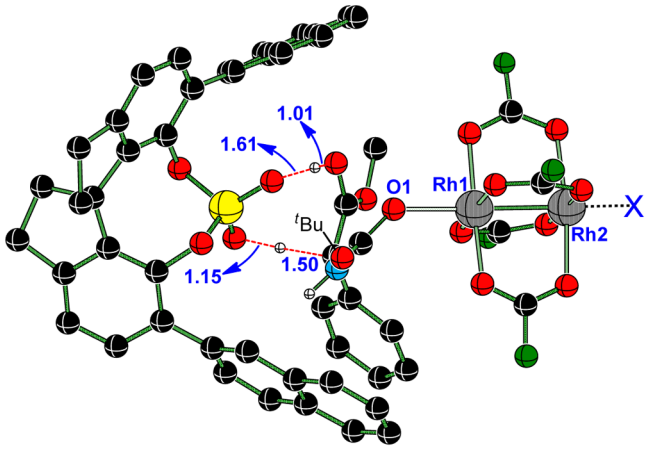

X	O1-Rh1	Rh1-Rh2	Rh2-X
-	2.26	2.43	-
(*R*)-SPA	2.37	2.44	2.31
NH_2Boc	2.38	2.45	2.27
$CHCl_3$	2.30	2.43	2.87

***si*-(5-6)‡···X**

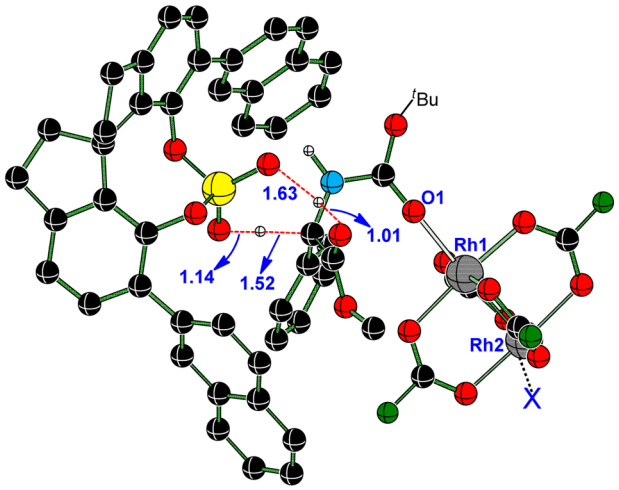

X	O1-Rh1	Rh1-Rh2	Rh2-X
-	2.30	2.43	-
(*R*)-SPA	2.40	2.45	2.31
NH_2Boc	2.41	2.45	2.27
$CHCl_3$	2.33	2.44	2.86

***re*-(5-6')‡···X**

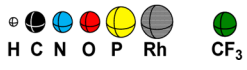

Figure 2. Optimized geometries of the stereocontrolling transition states for the asymmetric protonation of the α-carbon of the dirhodium-bound enol (**5···X**) by (*R*)-SPA. Where X is 0(Nil), $CHCl_3$, NH_2Boc and (*R*)-SPA. The distances are in Å optimized at the $SMD_{(chloroform)}$/M06/LanL2DZ(Rh),6-31G**//B3LYP/LanL2DZ-(Rh),6-31G* level of theory for TS when X is (*R*)-SPA. Only selected C and H are shown.

trends in the geometric changes in the stereocontrolling transition states are closely similar in both ***si*-(5−6)‡···(*R*)-SPA** and ***re*-(5−6)‡···(*R*)-SPA**, the O1−Rh1 distances are longer in the higher energy transition state involving the *re*-face protonation.

Table 2. Computed Relative Gibbs Free Energies[a] (in kcal/mol) in the Solvent Continuum for the Stereodetermining Transition States with and without Different Axial Ligands (X)

X	***si*-(5−6)‡···X**	***re*-(5−6′)‡···X**
–	−24.4	−17.0
(*R*)-SPA	−30.7	−24.0
NH_2Boc	−28.9	−24.1
$CHCl_3$	−19.0	−10.9

[a]The relative Gibbs free energies at the $SMD_{(chloroform)}$/M06/LanL2DZ(Rh),6-31G**(H,C,N,O,F,P,Cl)//B3LYP/LanL2DZ(Rh),6-31G*(H,C,N,O,F,P,Cl) level of theory are computed with respect to the separated reactants. The relative Gibbs free energies of intermediate **5···X** with respect to the separated reactants are −27.7, −29.5, −32.1, and −20.7, respectively, for X = Nil, (*R*)-SPA, NH_2Boc, and $CHCl_3$.

Analysis of interaction energies of various axial ligands (X) in the transition state with the dirhodium framework revealed that the strongest binding is with (*R*)-SPA and the weakest is with chloroform.[25] The stronger interaction with the axial ligand should be regarded as the source of additional stabilization of the transition state **(5−6)‡···(*R*)-SPA**. In fact, the computed relative enthalpies of the protonation transition states **(5−6)‡···X** indicate a systematic variation with **(5−6)‡···(*R*)-SPA** having the lowest enthalpy while that without the axial coordination exhibits the highest enthalpy.[26] In addition to these electronic features, an interesting hydrogen bonding stabilization is noticed between the acidic proton of the axial phosphoric acid with the oxygen atoms of the trifluoroacetate bridge.[27] The cumulative effect of the above-mentioned factors render additional stabilization to **(5−6)‡···(*R*)-SPA** as compared to when other ligands coordinate to the axial position.

CONCLUSIONS

The cooperative action of two catalysts, dirhodium(II) tetra(trifluoroacetate) and chiral spiro phosphoric acid (*R*)-SPA in an asymmetric N−H insertion reaction, has been established by using transition-state modeling. While the enthalpy of stabilization due to axial ligation has been found to be significant, the Gibbs free energy differences are rather modest. The Gibbs free energies of the transition state as well as the activation barriers in almost all the key steps exhibited no significant kinetic advantage due to axial ligation. This prediction is along similar lines to the earlier reports obtained through the solution phase equilibrium measurements. However, the stereocontrolling transition state for the enantioselective protonation enjoys additional stabilization due to the presence of an axial (*R*)-SPA. The barrier to protonation has also been lowered by the axial coordination of (*R*)-SPA. The predicted sense of enatioselectivity in favor of the *R* enantiomer has been found to be in good agreement with the experimental value. The key conclusion is that the axial ligation is not preferred in most of the steps due to an increase in the activation barriers, except in the enantioselective protonation.

ASSOCIATED CONTENT

Supporting Information

Optimized geometries of all stationary points, electronic energies, Gibbs free energies, and other relevant details (such as atoms-in-molecules, natural bond orbital analysis). This

DOI: 10.1021/jo5027029
J. Org. Chem. 2015, 80, 2192−2197

material is available free of charge via the Internet at http://pubs.acs.org.

AUTHOR INFORMATION

Corresponding Author

*E-mail: sunoj@chem.iitb.ac.in.

Notes

The authors declare no competing financial interest.

ACKNOWLEDGMENTS

Research funding from BRNS (Mumbai) under the basic sciences scheme and computing time from the IIT Bombay computer center and the National Nanotechnology Infrastructure Network at Michigan are gratefully acknowledged. A senior research fellowship (H.K.K.) from CSIR (New Delhi) is acknowledged.

REFERENCES

(1) (a) Davies, H. M. L. *Angew. Chem., Int. Ed.* **2006**, *45*, 6422. (b) Davies, H. M. L. *Angew. Chem., Int. Ed.* **2006**, *45*, 6422. (c) Hu, W.; Xu, X.; Zhou, J.; Liu, W.-J.; Huang, H.; Hu, J.; Yang, L.; Gong, L.-Z. *J. Am. Chem. Soc.* **2008**, *130*, 7782. (d) Davies, H. M. L.; Manning, J. R. *Nature* **2008**, *451*, 417. (e) Doyle, M. P.; Duffy, R.; Ratnikov, M.; Zhou, L. *Chem. Rev.* **2010**, *110*, 704. (f) Jiang, J.; Xu, H.-D.; Xi, J.-B.; Ren, B.-Y.; Lv, F.-P.; Guo, X.; Jiang, L.-Q.; Zhang, Z.-Y.; Hu, W.-H. *J. Am. Chem. Soc.* **2011**, *133*, 8428. (g) Xu, B.; Zhu, S.-F.; Xie, X.-L.; Shen, J.-J.; Zhou, Q.-L. *Angew. Chem., Int. Ed.* **2011**, *50*, 11483. (h) Wang, X.; Abrahams, Q. M.; Zavalij, P. Y.; Doyle, M. P. *Angew. Chem., Int. Ed.* **2012**, *51*, 5907. (i) Qiu, H.; Li, M.; Jiang, L.-Q.; Lv, F.-P.; Zan, L.; Zhai, C.-W.; Doyle, M. P.; Hu, W.-H. *Nat. Chem.* **2012**, *4*, 733. (j) Terada, M.; Toda, Y. *Angew. Chem., Int. Ed.* **2012**, *51*, 2.93. (k) Li, Z.; Boyarskikh, V.; Hansen, J. H.; Autschbach, J.; Musaev, D. G.; Davies, H. M. L. *J. Am. Chem. Soc.* **2012**, *134*, 15497. (l) Gulevich, A. V.; Gevorgyan, V. *Angew. Chem., Int. Ed.* **2013**, *52*, 1371. (m) Jat, J. L.; Paudyal, M. P.; Gao, H.; Xu, Q.-L.; Yousufuddin, M.; Devarajan, D.; Ess, D. H.; Kürti, L.; Falck, J. R. *Science* **2014**, *343*, 61.

(2) (a) Pirrung, M. C.; Liu, H.; Morehead, A. T., Jr. *J. Am. Chem. Soc.* **1996**, *118*, 8162. (b) Nakamura, E.; Yoshikai, N.; Yamanaka, M. *J. Am. Chem. Soc.* **2002**, *124*, 7181. (c) Nowlan, D. T., III; Gregg, T. M.; Davies, H. M. L.; Singleton, D. A. *J. Am. Chem. Soc.* **2003**, *125*, 15902. (d) Wong, F. M.; Wang, J.; Hengge, A. C.; Wu, W. *Org. Lett.* **2007**, *9*, 1663.

(3) (a) Chifotides, H. T.; Dunbar, K. R. Rhodium Compounds. In *Multiple Bonds between Metal Atoms*; Cotton, F. A., Murillo, C. A., Walton, R. A., Eds.; Springer Science and Business Media: New York, 2005; pp 465−567. (b) Timmons, D. J.; Doyle, M. P. Chiral Dirhodium(II) Catalysts and Their Applications. In *Multiple Bonds between Metal Atoms*; Cotton, F. A., Murillo, C. A., Walton, R. A., Eds.; Springer Science and Business Media: New York, 2005; pp 591−626.

(4) Cotton, F. A.; Dikarev, E. V.; Petrukhina, M. A. *J. Am. Chem. Soc.* **2001**, *123*, 11655.

(5) Petrukhina, M. A.; Andreini, K. W.; Peng, L.; Scott, L. T. *Angew. Chem., Int. Ed.* **2004**, *43*, 5477.

(6) Lebel, H.; Piras, H.; Bartholoméüs, J. *Angew. Chem., Int. Ed.* **2014**, *53*, 7300.

(7) (a) Gois, P. M. P.; Trindade, A. F.; Veiros, L. F.; André, V.; Duarte, M. T.; Afonso, C. A. M.; Caddick, S.; Cloke, F. G. N. *Angew. Chem., Int. Ed.* **2007**, *46*, 5750. (b) Trindade, A. F.; Gois, P. M. P.; Veiros, L. F.; André, V.; Duarte, M. T.; Afonso, C. A. M.; Caddick, S.; Cloke, F. G. N. *J. Org. Chem.* **2008**, *73*, 4076.

(8) Kornecki, K. P.; Briones, J. F.; Boyarskikh, V.; Fullilove, F.; Autschbach, J.; Schrote, K. E.; Lancaster, K. M.; Davies, H. M. L.; Berry, J. F. *Science* **2013**, *342*, 351.

(9) Doyle, M. P.; Winchester, W. R.; Hoorn, J. A. A.; Lynch, V.; Simonsen, S. H.; Ghosh, R. *J. Am. Chem. Soc.* **1993**, *115*, 9968.

(10) Drago, R. S.; Long, L. R.; Cosmano, R. *Inorg. Chem.* **1981**, *20*, 2920.

(11) Pirrung, M. C.; Liu, H.; Morehead, A. T., Jr. *J. Am. Chem. Soc.* **2002**, *124*, 1014.

(12) Xu, X.; Zavalij, P. Y.; Doyle, M. P. *J. Am. Chem. Soc.* **2013**, *135*, 12439.

(13) Lindsay, V. N. G.; Nicolas, C.; Charette, A. B. *J. Am. Chem. Soc.* **2011**, *133*, 8972.

(14) Mattiza, J. T.; Fohrer, J. G. G.; Duddeck, H.; Gardiner, M. G.; Ghanem, A. *Org. Biomol. Chem.* **2011**, *9*, 6542.

(15) (a) Anand, M.; Sunoj, R. B. *Org. Lett.* **2012**, *14*, 4584. (b) Jindal, G.; Sunoj, R. B. *J. Org. Chem.* **2014**, *79*, 7600. (c) Jindal, G.; Sunoj, R. B. *J. Am. Chem. Soc.* **2014**, *136*, 15998.

(16) Kisan, H. K.; Sunoj, R. B. *Chem. Commun.* **2014**, *50*, 14639.

(17) All computations were performed using Gaussian 09, Revision A.02: Frisch, M. J.; Trucks, G. W.; Schlegel, H. B.; Scuseria, G. E.; Robb, M. A.; Cheeseman, J. R.; Scalmani, G.; Barone, V.; Mennucci, B.; Petersson, G. A.; Nakatsuji, H.; Caricato, M.; Li, X.; Hratchian, H. P.; Izmaylov, A. F.; Bloino, J.; Zheng, G.; Sonnenberg, J. L.; Hada, M.; Ehara, M.; Toyota, K.; Fukuda, R.; Hasegawa, J.; Ishida, M.; Nakajima, T.; Honda, Y.; Kitao, O.; Nakai, H.; Vreven, T.; Montgomery, J. A., Jr.; Peralta, J. E.; Ogliaro, F.; Bearpark, M.; Heyd, J. J.; Brothers, E.; Kudin, K. N.; Staroverov, V. N.; Kobayashi, R.; Normand, J.; Raghavachari, K.; Rendell, A.; Burant, J. C.; Iyengar, S. S.; Tomasi, J.; Cossi, M.; Rega, N.; Millam, N. J.; Klene, M.; Knox, J. E.; Cross, J. B.; Bakken, V.; Adamo, C.; Jaramillo, J.; Gomperts, R.; Stratmann, R. E.; Yazyev, O.; Austin, A. J.; Cammi, R.; Pomelli, C.; Ochterski, J. W.; Martin, R. L.; Morokuma, K.; Zakrzewski, V. G.; Voth, G. A.; Salvador, P.; Dannenberg, J. J.; Dapprich, S.; Daniels, A. D.; Farkas, Ö.; Foresman, J. B.; Ortiz, J. V.; Cioslowski, J.; Fox, D. J. Gaussian, Inc., Wallingford CT, 2009.

(18) (a) Becke, A. D. *Phys. Rev. A* **1988**, *38*, 3098. (b) Becke, A. D. *J. Chem. Phys.* **1993**, *98*, 5648. (c) Lee, C.; Yang, W.; Parr, R. G. *Phys. Rev. B* **1998**, *37*, 785.

(19) (a) Hay, P. J.; Wadt, W. R. *J. Chem. Phys.* **1985**, *82*, 299. (b) Hehre, W. J.; Ditchfield, R.; Pople, J. A. *J. Chem. Phys.* **1972**, *56*, 2257. (c) Hariharan, P. C.; Pople, J. A. *Theor. Chim. Acta.* **1973**, *28*, 213.

(20) (a) Gonzalez, C.; Schlegel, H. B. *J. Chem. Phys.* **1989**, *90*, 2154. (b) Gonzalez, C.; Schlegel, H. B. *J. Phys. Chem.* **1990**, *94*, 5523.

(21) Marenich, A. V.; Cramer, C. J.; Truhlar, D. G. *J. Phys. Chem. B* **2009**, *113*, 6378.

(22) (a) Reed, A. E.; Weinstock, R. B.; Weinhold, F. *J. Chem. Phys.* **1985**, *83*, 735. (b) Reed, A. E.; Curtiss, L. A.; Weinhold, F. *Chem. Rev.* **1988**, *88*, 899. (c) Glendening, E. D.; Reed, A. E.; Carpenter, J. E.; Weinhold, F. NBO Version 3.1; Gaussian, Inc.: Wallingford, CT, 2009.

(23) (a) Davies, H. M. L.; Venkataramani, C. *Org. Lett.* **2003**, *5*, 1403. (b) Trindade, A. F.; Coelho, J. A. S.; Afonso, C. A. M.; Veiros, L. F.; Gois, P. M. P. *ACS Catal.* **2012**, *2*, 370.

(24) See Figure S1 (Supporting Information) for additional details on conformational analysis of the stereodetermining transition states.

(25) See Table S1 (Supporting Information).

(26) See Table S2 (Supporting Information).

(27) See Figure S2 and Table S3 (Supporting Information) for a summary of NBO analysis and geometric details.

DOI: 10.1021/jo5027029
J. Org. Chem. 2015, 80, 2192−2197